Dispenser-printed planar thick-film thermoelectric energy generators

2011 J. Micromech. Microeng. 21 104006

(http://iopscience.iop.org/0960-1317/21/10/104006)

J. Micromech. Microeng. **21** (2011) 104006 (8pp) doi:10.1088/0960-1317/21/10/104006

Dispenser-printed planar thick-film thermoelectric energy generators

A Chen[1], D Madan[1], P K Wright[1] and J W Evans[2]

[1] Department of Mechanical Engineering, University of California, Berkeley, CA, USA
[2] Department of Materials Science & Engineering, University of California, Berkeley, CA, USA

E-mail: alic.chen@berkeley.edu

Received 1 April 2011, in final form 26 May 2011
Published 29 September 2011
Online at stacks.iop.org/JMM/21/104006

Abstract
This work presents advancements in dispenser-printed thick film thermoelectric materials for the fabrication of planar and printable thermoelectric energy generators. The thermoelectric properties of the printed thermoelectric materials were measured as a function of temperature. The maximum dimensionless figures of merit (ZTs) at 302 K for the n-type Bi_2Te_3-epoxy composite and the p-type Sb_2Te_3-epoxy composite are 0.18 and 0.19, respectively. A 50-couple prototype with 5 mm $\times$ 640 μm $\times$ 90 μm printed element dimensions was fabricated on a polyimide substrate with evaporated metal contacts. The prototype device produced a power output of 10.5 μW at 61.3 μA and 171.6 mV for a temperature difference of 20 K resulting in a device areal power density of 75 μW cm^{-2}.

(Some figures in this article are in colour only in the electronic version)

1. Introduction

Thermoelectric energy generators (TEGs) have potential applications for waste heat recovery, remote power generation or autonomous microsystems. Thermoelectric power generation provides solid-state conversion of heat into electrical power by utilizing the Seebeck effect. When a temperature difference is applied across a thermoelectric generator, a voltage can be measured and converted into dc power [1]. TEGs have great appeal due to their solid-state nature as they are silent, require no moving parts and have proven reliability through extended use [2]. While the bulk of thermoelectric research has focused on the synthesis of novel and efficient materials [3, 4], there has been less attention to device-level manufacturing.

Thermoelectric devices consist of alternating n-type and p-type semiconductor elements placed electrically in series and thermally in parallel. Figure 1(*a*) shows a schematic of a typical thermoelectric device design. Efficient TEGs for small-scale energy generation require fabrication of high-aspect-ratio semiconductor elements in high-density arrays [5–7]. Conventional three-dimensional TEG designs are however frequently limited to low-aspect-ratio elements due to manufacturing limitations. Moreover, bulk-manufacturing techniques cannot achieve these TEG design requirements in a scalable and cost-effective manner. Alternatively, by utilizing a planar device design, high-density and therefore higher efficiency TEGs can be fabricated on electrically insulating substrates [7–9]. Flexible substrates enable planar high-density array devices to be rolled into a compact form factor as shown in figure 1(*b*) [9]. Films deposited on flexible substrates, however, require long fatigue life to prevent cracking [10]. Such devices are difficult to produce using standard microfabrication methods due to limitations in evaporation and sputtering techniques.

Printed thick-film deposition techniques are well suited for fabrication and material requirements of flexible planar TEG devices. Printing involves the deposition of thermoelectric inks that are synthesized by mixing active materials in polymer binders and solvents [11–14]. The energy input and waste generated in printing are both reduced substantially compared to thin-film microfabrication procedures [15–17]. Printing methods are also scalable to other mass manufacturing printing practices including screen printing and flexography. We have previously proposed methods for the development of thermoelectric materials and devices using dispenser printing [11, 18, 19].

This work presents the development of unique printable composite thermoelectric systems optimized for low-temperature applications. While previous work has focused on

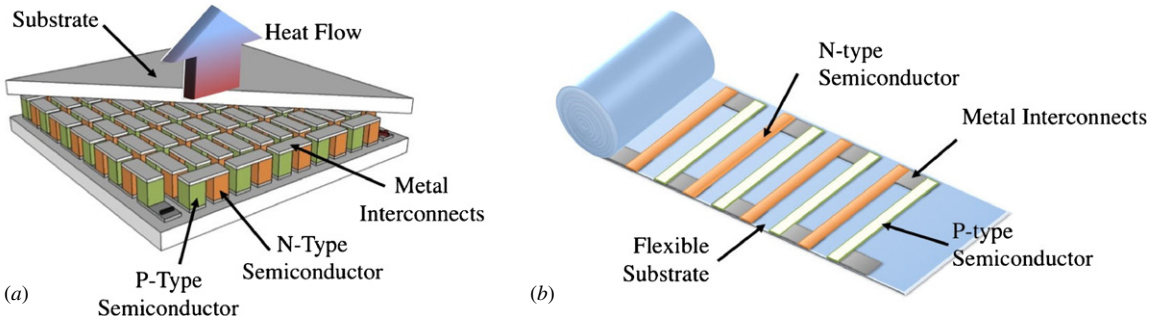

Figure 1. Schematic of a planar thermoelectric device with printed active elements.

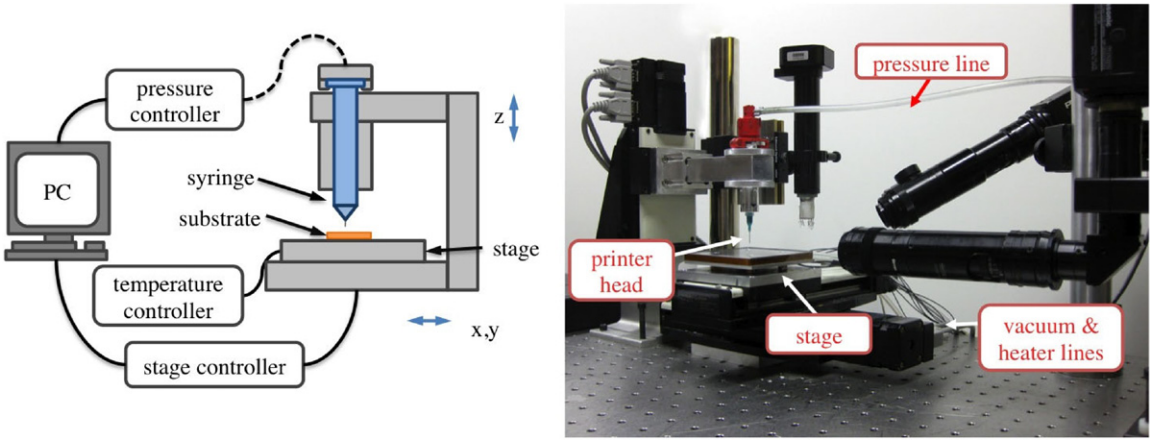

Figure 2. Left: schematic of the dispenser printer, and right: image of the dispenser printer.

optimization and characterization of printable thermoelectric materials, this work demonstrates and characterizes the first reported dispenser-printed planar TEG for low-temperature energy harvesting applications.

2. Experimental details

2.1. Dispenser printing

The prototyping dispenser printer used in this work consists of a three-axis stage, a pneumatically controlled dispensing syringe head and a heated vacuum chuck stage. Figure 2 shows an image and schematic of the dispenser printer. The printer stages are Newmark Systems NLS4 series stages with 0.03 μm resolution and 5 μm repeatability (based on manufacturer's specifications). The stage controller is a Newmark Systems MSC-M four-axis stage controller and has 1 μm resolution (based on the manufacturer's specifications). Side-view and angled-view cameras are used to image the printer tip relative to the substrate. A top-down camera is used for custom-developed automated software alignment of the dispensing tip. The printer allows for deposition of inks of a wide range of viscosities from 100–10 000 cP, and is controlled using a Musashi ML-808FX pneumatic controller capable of 20–500 kPa output. All equipment is interfaced and controlled through a personal computer running custom Java software. Depending on the inks, typical feature sizes down to 50 μm can be printed with film thicknesses ranging from 10 to 200 μm per pass, depending on a combination of process parameters such as shot pressure, tip size, rheology of the ink and shot spacing. These parameters are all easily tuned within the automated software and allow for rapid adjustments to the process parameters in real time. Ink viscosity can be tuned by adjusting the amount of solvent/diluent in the mixture (which is removed upon drying), while tip sizes are adjusted by using commercially available disposable plastic and metal syringe tips. These tips are available in sizes ranging from several mm down to 100 μm in inner diameter, and smaller tips under 100 μm in inner diameter can be manually pulled from borosilicate glass pipettes. Thermoelectric heater/coolers below the stage allow for heating or cooling of substrate for on-contact drying.

This prototype dispenser printer has been previously used in various other research projects including printed solid-state energy storage devices [20, 21], MEMS AC current sensors [22] and MEMS vibrational energy harvesting [23].

2.2. Material synthesis

The printable thermoelectric materials are composite systems, consisting of active thermoelectric powder (n-type Bi_2Te_3 or p-type Sb_2Te_3 particles) and a polymer binder. Empirical testing has suggested that powders with an average particle size of 10 μm produce optimal composite properties [18, 24, 25]. To synthesize such powders, 80–100 mesh Bi_2Te_3 (Merit Technology Group Co., Ltd) and Sb_2Te_3 (Super Conductor

Materials, Inc.) powders were individually placed into 100 ml stainless steel jars with 3 mm stainless steel balls at a ball-to-powder mass ratio of 10:1. The jars were then placed in a high-energy planetary ball mill (Torrey Hills ND 0.4L) and operated at rotational speeds of 210–280 rpm for 30–180 min. Isopropanol (Sigma Aldrich, Inc.) was used as a process control agent at a 1:1 weight ratio of powder to fluid. All material preparation and extraction were performed in a dry argon environment to prevent the oxidation of materials. The particle size distribution of the powders was confirmed using a Coulter LS-100 particle sizer. The resulting average particle size after ball milling was 10 μm while the particles ranged between 2 and 60 μm.

The polymer binder was an epoxy system formulated using a bisphenol f epoxy resin (EPON 862, Hexion Specialty Chemicals, Inc.) and an anhydride-based hardener (MHHPA, Broadview Technologies, Inc.). The epoxy-to-hardener equivalent weight ratio was 1:0.85. A phosphate-based accelerator (AC-8, Broadview Technologies, Inc.) was employed as the catalyst in the system. 10–20 wt% of butyl glycidyl ether (Heloxy 61, Hexion Specialty Chemicals, Inc.) was added to the resin blend as a reactive diluent to reduce the viscosity of the ink. Low percentages of organic solvents were also used to both extend the pot-life of the epoxy system and adjust the viscosity for printing. The epoxy system used in this work was particularly chosen for its low viscosity and extended pot-life [24, 25]. The viscosity of the formulated inks is acceptable for thick-film printing processes such as dispensing printing, screen-printing and roll-to-roll flexographic printing. However, the ink can be formulated for lower viscosity printing methods such as ink-jet printing or spray deposition through addition of more diluents.

80–82 wt% Bi_2Te_3 or Sb_2Te_3 powder and 18–20 wt% epoxy resin were mixed to make inks. The inks were mixed using a vortex mixer and an ultrasonic bath to disperse the particles. The thermoelectric inks were then printed on glass substrates to form 100–200 μm thick films using the dispenser printer. The films were finally cured at 250 °C either in an argon or vacuum oven for a minimum of 3 h. Previous studies have described the effects of processing and optimization of these thermoelectric composite inks [11]. Figure 3 shows a scanning electron microscope image of a dispenser-printed Bi_2Te_3/epoxy composite film cured at 250 °C. The images suggest that the composite films are uniform and have low porosity.

Bulk samples of the Sb_2Te_3 powders were additionally synthesized using traditional cold-pressing techniques [11]. These samples were used for comparison of material properties relative to the composite films. Bulk samples of Bi_2Te_3 from the stock batch were used as the reference material for the n-type composite film.

2.3. Device fabrication

Figure 4 shows an envisioned manufacturing process for dispenser-printed planar thermoelectric devices. In this work, each individual step was performed as a batch process with a stationary substrate. Gold metal contacts were first deposited via shadow mask evaporation onto a 50.8 μm thick flexible polyimide substrate. Polyimide is an ideal substrate due to its flexibility, electrical insulation, high temperature tolerance and low thermal conductivity (0.12 W m^{-1} K^{-1}). Next, the individual n-type and p-type elements were dispenser printed onto the substrate to form lines spanning across the top and bottom contacts. The printed lines were then cured in an argon oven at 250 °C. Figure 5(*a*) shows a picture of the printed thermoelectric lines on a flexible polyimide sheet with evaporated contacts. Printed devices were cut out of the polyimide sheet. 24 AWG copper wires were attached to the device using conductive silver epoxy (1901-S, ESL Electroscience) to form electrical connections. Finally, the device was completed by rolling the substrate to form a coil and sealed with polyimide tape. Figure 5(*b*) shows a 50-couple prototype consisting of elements that were 5 mm × 640 μm × 90 μm with 360 μm element spacing. Testing and characterization of the prototype will be discussed later.

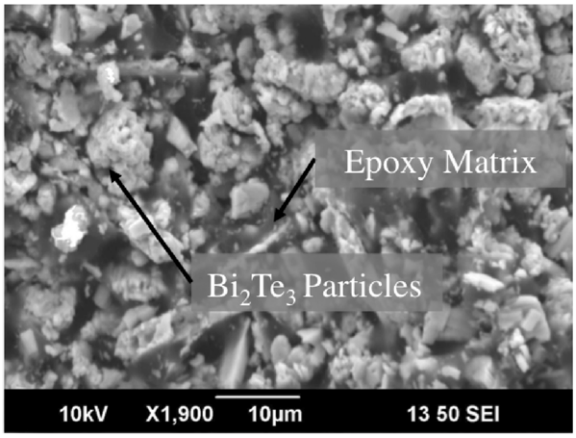

Figure 3. Scanning electron microscope image of Bi_2Te_3/epoxy composite film cured at 250 °C.

2.4. Material and device characterization

The primary material properties of interest are the electrical conductivity (σ), the Seebeck coefficient (α) and the thermal conductivity (λ). These material properties are the constituent variables for the widely used thermoelectric figure of merit (ZT):

$$ZT = \frac{\alpha^2 \sigma}{\lambda} T, \tag{1}$$

where T is the temperature. State-of-the-art ZT materials have ZT$\sim$1, while the recent advances in novel materials have reached ZT values of up to 2.5 [3, 4]. Electrical conductivity measurements of the printed thermoelectric materials were carried out using the Van der Pauw method to determine the sheet resistance of the materials. Seebeck measurements were performed using a custom Seebeck testing system to determine the voltage output of the material for a given temperature difference (ΔT). Both the electrical conductivity and the Seebeck coefficients of the materials were measured at various temperature set points

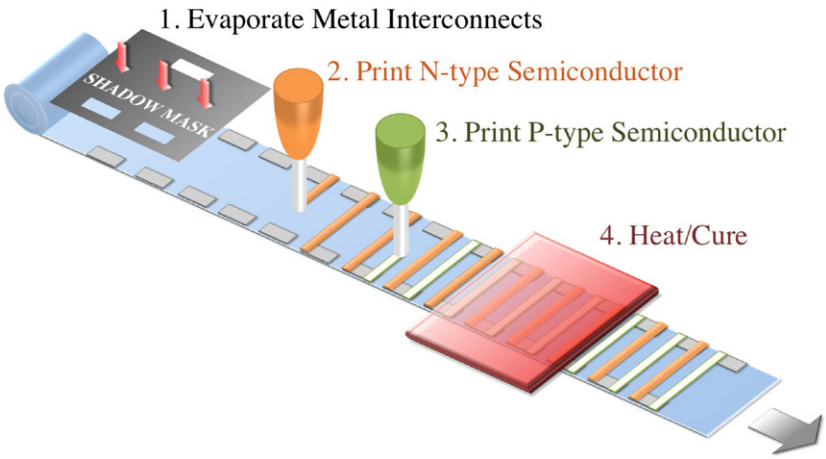

Figure 4. Fabrication process for a planer dispenser-printed thermoelectric device.

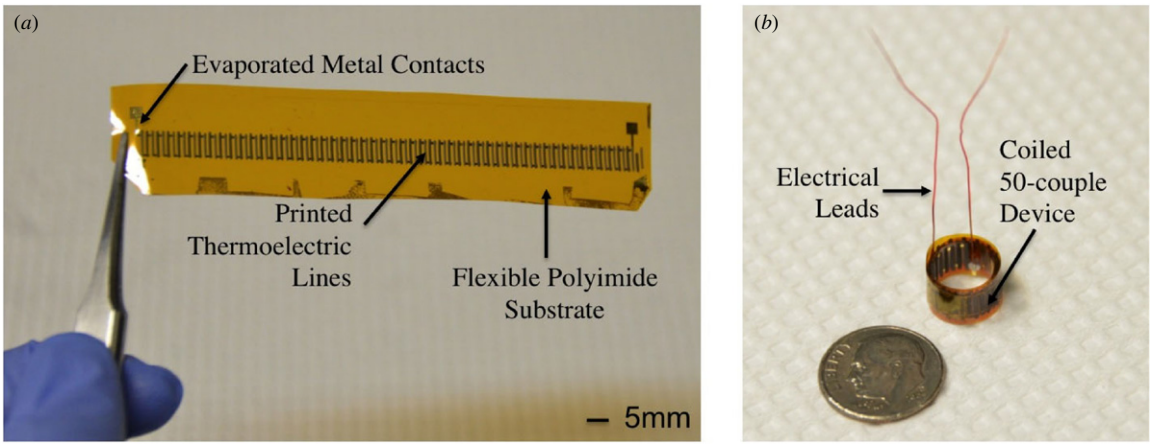

Figure 5. Images of (*a*) printed 50-couple planar thermoelectric device on a flexible polyimide substrate and (*b*) coiled prototype with electrical connections.

ranging from room temperature to 150 °C. This allows for material characterization at temperature ranges of low-grade heat applications. For each temperature set point, up to 70 measurements were taken for each sample. All measurements were taken in an insulated Faraday cage to limit sources of error from the ambient environment. Thermal conductivity measurements were performed using an Anter Corp. Model 2021 steady-state thermal conductivity tester. Measurements of thermal conductivity were limited by the large sample size requirements (25.4 mm × 25.4 mm) of the tester. Large composite samples were prepared by first casting the thermoelectric slurries in a Teflon mold. The mold was then similarly cured in an argon/vacuum oven.

The printed prototype device was tested by placing the device on a heater while carefully monitoring the temperature at both ends of the elements with thermocouples mounted with thermal joint compound (TIM-417, Wakefield Solutions). Once the device reached steady state, the open circuit voltage of the device was measured using a digital multimeter. A variable load resistance was then connected in series with the device and voltage measurements were taken at multiple load resistances. The power was then calculated based on the measured voltage and load resistance at various temperature differences.

3. Results

3.1. Composite thermoelectric materials

Figure 6 shows the temperature dependence of the thermoelectric composite materials compared to the values of bulk cold-pressed samples. The Seebeck coefficient (α) of the p-type Sb_2Te_3 composite has a peak value of approximately 160 μV K^{-1} when cured at 250 °C, which is higher than the bulk cold-pressed Sb_2Te_3. However, the electrical conductivity (σ) of the composite system is approximately an order of magnitude less than that of bulk sample. This is due to the insulating characteristics of the polymer. Previous studies have shown that the particles in the p-type Sb_2Te_3 composite sinter when cured at 350 °C [11]. This allows for better hole transport and increases σ for the composite by an order of magnitude [26]. Although the resulting power factor ($\alpha^2\sigma$) for the sintered Sb_2Te_3 composite may be higher, the

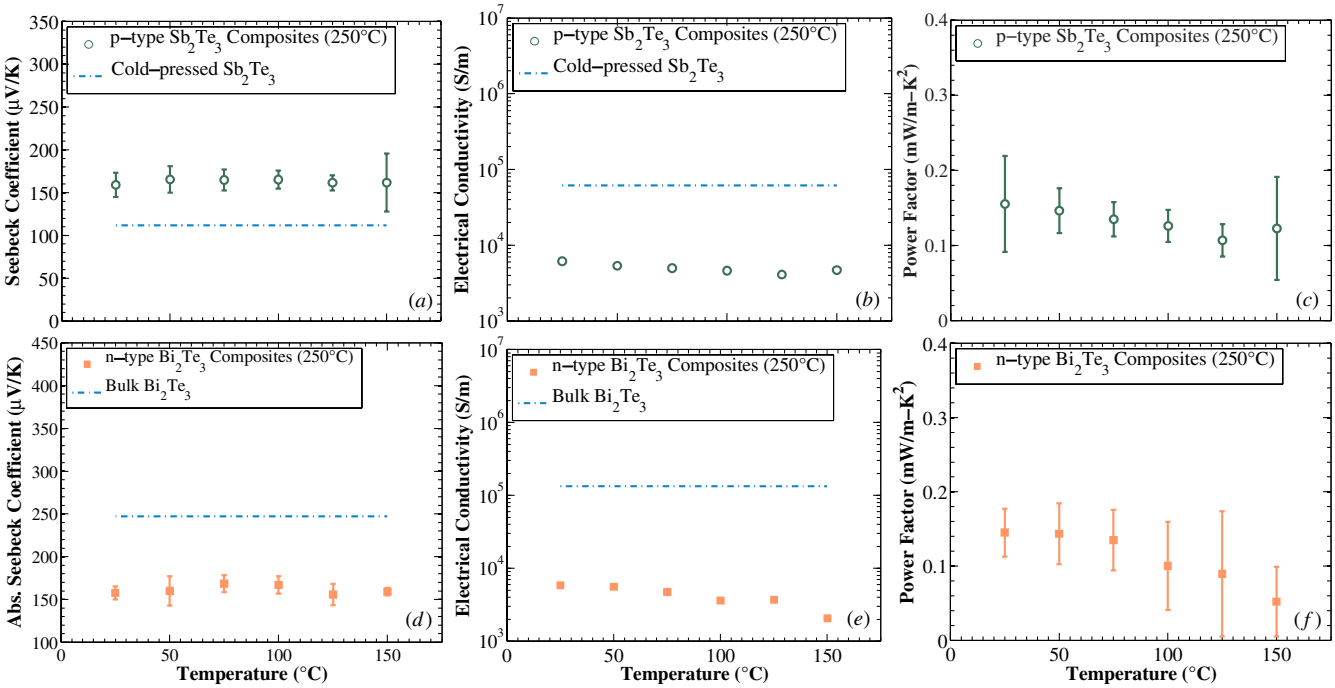

Figure 6. Temperature dependence of the (*a*), (*d*) Seebeck coefficient, (*b*), (*e*) electrical conductivity and (*c*), (*f*) power factor for Bi_2Te_3 composites (solid square) and Sb_2Te_3 composites cured at 250°C (clear circle).

implications of a higher curing temperature for a printed device require further investigation.

Sintering of the n-type Bi_2Te_3 composite was not achievable because its high temperature sintering requirements exceed the 400 °C disintegration temperature of the polymer. The α of the Bi_2Te_3 composite n-type system cured at 250 °C is -157 μV K^{-1}, comparable to that of the p-type Sb_2Te_3. However, the σ of the Bi_2Te_3 composite is almost two orders of magnitude lower than that of bulk due to the insulating polymer in the system.

The temperature dependence of the composite materials suggests that the materials are best suited for near-room-temperature applications. Both composite systems show a decreasing trend in performance as the operating temperature increases. These trends in power factor are similar to those of bismuth and antimony telluride-based materials [27]. Further research involving processing, optimization and low-temperature sintering additives is currently being explored to improve the performance of these composites.

Table 1 shows the thermal conductivity and maximum dimensionless figure of merit (ZT) values of the various composite thermoelectric materials at room temperature. Both the Sb_2Te_3 and Bi_2Te_3 systems exhibit low thermal conductivities due to the insulating effects of the polymer. The resulting ZT's of the Sb_2Te_3 and the Bi_2Te_3 composites reach 0.19 and 0.18, respectively.

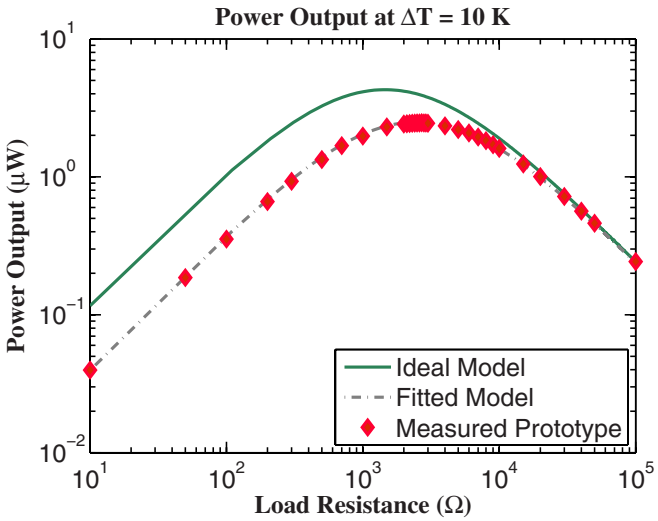

Figure 7. Power output of the 50-couple prototype generator as a function of load resistance at a 10 K temperature difference.

Table 1. Thermal conductivity and ZT values for composite thermoelectric materials.

Composite material	Curing temp.	Thermal conductivity (W m^{-1} K^{-1})	ZT
p-type Sb_2Te_3	250 °C	0.24	0.19
n-type Bi_2Te_3	250 °C	0.24	0.18

3.2. Prototype device characterization

The initial measured device resistance of the prototype was 2.3 kΩ. However, after coiling and packaging, the device resistance increased to 2.55 kΩ. This is likely due to some internal strain in the printed material and the contact interface during coiling [28]. Figure 7 shows the power output of the 50-couple prototype measured for $\Delta T = 10$ K at various load resistances. The optimal power output of the device

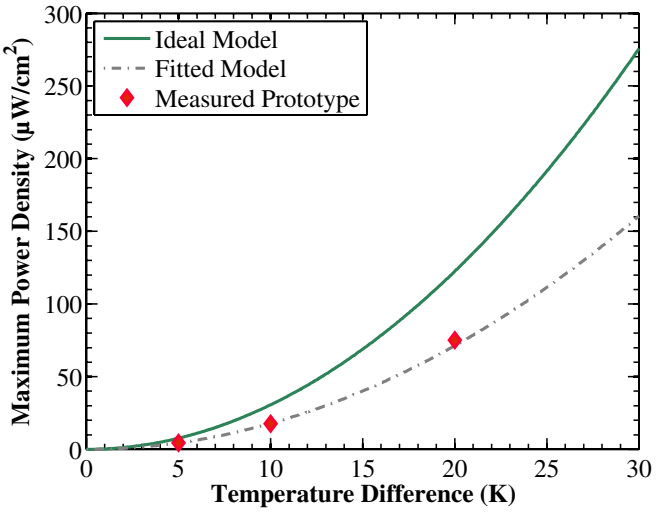

Figure 8. Maximum power output at matched load resistance as a function of temperature difference across the generator for the ideal generator model (solid line), the measured prototype (solid diamonds) and the fitted model (dashed line).

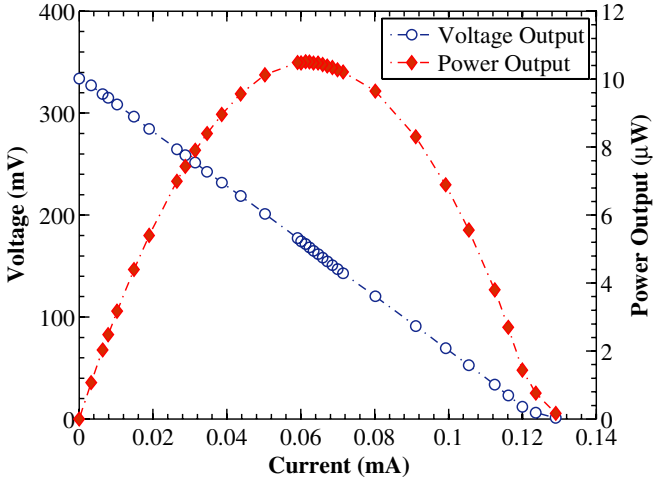

Figure 9. Characteristic curve for the 50-couple coiled generator at $\Delta T = 20$ K.

occurs when the load resistance matches the device resistance. The device resistance, however, is higher than the expected resistance calculated from the material properties. The solid line in figure 7 indicates the ideal power output based on the general thermoelectric power model [5, 6, 29], while the dashed line indicates the fitted model for the device. The general thermoelectric power model can be described as

$$P = \frac{(m\alpha_{n+p}\Delta T)^2}{4R_{\text{gen}}}, \tag{2}$$

where m is the number of couples, α_{n+p} is the Seebeck coefficient of a couple, ΔT is the temperature differences and R_{gen} is the generator resistance. In the ideal scenario, the generator resistance can be estimated as

$$R_{\text{gen}} = 2m\rho_m \frac{L}{A}, \tag{3}$$

where ρ_m is the electrical resistivity of the material, L is the element length in the direction of heat flow and A is the cross-sectional area of the element. In the case of the fitted model, R_{gen} was the measured resistance of the generator. The measured data for the prototype closely matches the fitted model suggesting that the Seebeck voltage output of the device aligns with the measured material properties. Error in the fit can be attributed to temperature oscillations during measurement.

Figure 8 shows the measured power density of the device as a function of the temperature difference. The maximum power output at matched load resistance was measured at ΔT of 5, 10 and 20 K. The solid line in figure 8 again indicates the ideal model, while the dashed line indicates the fitted model based on the equations described above. Figure 9 shows the device characteristic curves for the prototype device at $\Delta T = 20$ K. At matched load resistance, the device produces approximately 10.5 μW at 61.3 μA and 171.6 mV.

4. Discussion

While the efficiency of printed thermoelectric composites is not as high as that of some state-of-the-art materials with ZT $\geqslant$ 1, the results are encouraging. The ease of processing and device fabrication with printed materials provides deployment advantages over such materials. Further material processing parameters may be able to improve the effective ZT of the materials and future work includes various materials' optimization.

The prototype in this work currently has a less than ideal electrical impedance, which is likely due to the electrical contact resistance between the printed films and metal contacts [25]. Examination of the metal/composite interface may provide solutions to reduce the resistance. Empirical studies have also suggested that the thickness of the metal contacts may affect the device resistance. The total device resistance can also be lowered through curing of the materials at higher temperatures as suggested by previous works [11]. Thermal expansion of the substrate and materials, however, must be considered at such temperatures since changes in volume will affect the coiling and packaging of the device. The 50-couple prototype presented in this work produced 10.5 μW for a 20 K temperature difference, yielding a cross-sectional areal power density of 75 μW cm^{-2}. This is well suited to scale for many low-power residential, industrial and medical wireless sensor applications [8, 30–35]. The modeling suggests that a device with current material properties is capable of achieving a power density of 109 μW cm^{-2} given negligible contact resistance. Thus, optimization of device design, fabrication and material processing will be further investigated to improve device performance. It is worth noting that in the case of a planar TEG design, the substrate reduces the effective heat flow through the active material [8, 9]. The choice of a thin and low thermal conductivity substrate, such as the polyimide used in this work, minimizes such losses.

The use of polymer-based systems as printed thermoelectric materials for TEGs is limited to low-grade heat (<200 °C) energy generation due to the polymer degradation

temperature [11]. These applications may include low-grade waste heat recovery [32], wearable electronics [33] or autonomous wireless sensor networks [34, 35]. While the TEG shown in this work demonstrates the feasibility of printed planar TEGs, the device has not been optimized for a specific application. However, the versatility of printed fabrication processes allows for rapid customization by varying the printed element length, width and thickness through printing parameter. Future work will include device design optimization and integration for low-temperature energy generation applications.

5. Conclusion

In this work, we have successfully synthesized printable thick-film thermoelectric materials for fabrication of planar high-density array and high-aspect-ratio TEGs. Material processing and optimization yield ZTs of 0.19 and 0.18 for p-type and n-type composites, respectively. A 50-couple planar prototype device was printed on a flexible polyimide substrate and rolled to form a coiled thermoelectric generator. The device produced 10.5 μW at 171.6 mV for a 20 K temperature difference with primary losses from device resistance. These results indicate an areal power density of 75 μW cm^{-2}. Further work will continue to optimize materials and device design for various applications. The results shown are promising for use of low-cost and scalable TEGs for various low-power energy harvesting applications.

Acknowledgments

The authors thank the California Energy Commission for supporting this research under contract 500-01-43. We also thank Brian Mahlstedt, Christine Ho, Jonathan Brown, Kevin Huang, Rei-Cheng Juang, Michael Nill and Mike Koplow for their contributions.

References

[1] Rowe D M 2005 *Thermoelectrics Handbook: Micro to Nano* (Boca Raton, FL: Taylor and Francis)
[2] Bell L E 2008 Cooling, heating, generating power, and recovering waste heat with thermoelectric systems *Science* **321** 1457–61
[3] Majumdar A 2004 Thermoelectricity in semiconductor nanosctructure *Science* **303** 777–8
[4] Vineis C J, Shakouri A, Majumdar A and Kanatzidis A 2010 *Adv. Mater.* **22** 3970–80
[5] Glatz W, Muntwyler S and Hierold C 2006 Optimization and fabrication of thick flexible polymer based micro thermoelectric generator *Sensors Actuators* A **132** 337–45
[6] Strasser M, Aigner R, Lauterbach C, Sturm T F, Franosch M and Wachutka G 2004 Micromachined CMOS thermoelectric generators as on-chip power supply *Sensors Actuators* A **114** 362–70
[7] Glatz W, Schwyter E, Durrer L and Hierold C 2009 Bi_2Te_3-based flexible micro thermoelectric generator with optimized design *J. Micromech. Syst.* **18** 763–72
[8] Hudak N S and Amatucci G G 2008 Small-scale energy harvesting through thermoelectric, vibration, and radiofrequency power conversion *J. Appl. Phys.* **103** 101301
[9] Weber J, Potje-Kamloth K, Haase F, Detemple P, Volklein F and Doll T 2006 Coin-size coiled-up polymer foil thermoelectric power generator for wearable electronics *Sensors Actuators* A **132** 325–30
[10] Gilleo K 1996 *Polymer Thick Film* (New York: Thomson Publishing)
[11] Madan D, Chen A, Wright P K and Evans J W 2011 Dispenser printed composite thermoelectric thick films for thermoelectric generator applications *J. Appl. Phys.* **109** 034904
[12] See K C, Feser J P, Chen C E, Majumdar A, Urban J J and Segalman R A 2010 Water-processable polymer−nanocrystal hybrids for thermoelectrics *Nano Lett.* **10** 4664–7
[13] Zhang B, Sun J, Katz H E, Fang F and Opila R L 2010 Promising thermoelectric properties of commercial PEDOT:PSS materials and their Bi_2Te_3 powder composites *ACS Appl. Mater. Interfaces* **2** 3170–8
[14] Navone C, Soulier M, Plissonnier M and Seiler A L 2009 Development of $(Bi,Sb)_2(Te,Se)_3$-based thermoelectric modules by a screen-printing process *J. Electron. Mater.* **39** 1755–9
[15] Hon K K B, Li L and Hutchings I M 2008 Direct write technology—advances and developments *CIRP Ann.—Manuf. Technol.* **57** 601–20
[16] Lewis J A and Gratson G 2004 Direct writing in three dimensions *Mater. Today* **7** 32–9
[17] Wright P K, Dornfeld D A, Chen A, Ho C C and Evans J W 2010 Dispenser printing for prototyping microscale devices *Trans. NAMRI/SME* **38** 555–61
[18] Chen A, Koplow M, Madan D, Wright P K and Evans J W 2009 *ASME Int. Mechanical Engineering Congress and Exposition (Lake Buena Vista, FL, 13–19 November 2009)* vol 13 p 11636
[19] Chen A, Madan D, Koplow M, Wright P K and Evans J W 2009 Dispenser printed thermoelectric generators *Technical Digest PowerMEMS 2009 (Washington, DC, USA, 1–4 December)* pp 277–80
[20] Ho C C, Evans J W and Wright P K 2010 Direct write dispenser printing of a zinc microbattery with an ionic liquid gel electrolyte *J. Micromech. Microeng.* **20** 104009
[21] Ho C C, Steingart D A, Salminen J P, Sin W H, Rantala T M K, Evans J W and Wright P K 2006 Dispenser printed electrochemical capacitors for power management of millimeter scale lithium ion polymer microbatteries for wireless sensors *Proc. 6th Int. Workshop on Micro and Nanotechnology for Power Generation and Energy* pp 219–22
[22] Leland E S, Wright P K and White R M 2009 A MEMS AC current sensor for residential and commercial electricity end-use monitoring *J. Micromech. Microeng.* **19** 094018
[23] Miller L M, Chen A, Wright P K and Evans J W 2010 Resonance frequency modification of MEMS vibration energy harvesters using dispenser-printed proof mass *Technical Digest PowerMEMS 2010 (Leuven, Belgium, 1–3 December)* pp 411–4
[24] Li Y and Wong C P 2006 Recent advances of conductive adhesives as a lead-free alternative in electronic packaging: materials, processing, reliability and applications *Mater. Sci. Eng.* R **51** 1–35
[25] Lu D and Wong C P 2000 A study of contact resistance of conductive adhesives based on anhydride-cured epoxy systems *IEEE Trans. Compon. Packag. Tech.* **23** 440–6

[26] Keawprak N, Sun Z M, Hashimoto H and Barsoum M W Effect of sintering temperature on the thermoelectric properties of pulse discharge sintered $(Bi_{0.24}Sb_{0.76})_2Te_3$ alloy *J. Alloys Compounds* **397** 236–44

[27] Poudel B *et al* 2008 High-thermoelectric performance of nanostructured bismuth antimony telluride bulk alloys *Science* **320** 634–8

[28] Cairns D R, Witte R P, Sparacin D K, Sachsman S M, Paine D C, Crawford G P and Newton R R 2000 Strain-dependent electrical resistance of tin-doped indium oxide on polymer substrates *Appl. Phys. Lett.* **176** 1425

[29] Rowe D M and Min G 1996 Design theory of thermoelectric modules for electrical power generation *IEE Proc., Sci. Meas. Technol.* **143** 351–6

[30] Ho C C, Mark M, Miller L, Chen A, Koplow M, Reilly E, Evans J W, Rabaey J and Wright P K 2009 Technologies for an autonomous home healthcare system *Proc. 6th Int. Workshop on Wearable and Implantable Body Sensor Networks* pp 29–34

[31] Pletcher N M, Gambini S and Rabaey J 2009 A 52μW wake-up receiver with sensitivity using an uncertain-IF architecture *IEEE J. Solid-Sate Circuits* **44** 269

[32] Rowe D M 2006 Thermoelectric waste heat recovery as a renewable energy source *Int. J. Innov. Energy Syst. Power* **1** 13–23

[33] Leonov V, Hoof C V and Vullers R J M 2009 Thermoelectric and hybrid generators in wearable devices and clothes *6th Int. Workshop on Wearable and Implantable Body Sensor Networks* pp 195–200

[34] Knight C and Davidson J 2010 Thermoelectric energy harvesting as a wireless sensor node power source *Proc. SPIE* **7643** 76431

[35] James E P *et al* 2004 An investigation of self-powered systems for condition monitoring applications *Sensors Actuators* A **110** 171–6